Journal of the Mechanical Behavior of Biomedical Materials 91 (2019) 345–354

Contents lists available at ScienceDirect

Journal of the Mechanical Behavior of Biomedical Materials

journal homepage: www.elsevier.com/locate/jmbbm

Mechanical properties of Bio-Ferrography isolated cancerous cells studied by atomic force microscopy

David Svetlizky[a], Ofer Levi[a], Itai Benhar[b], Noam Eliaz[a,*]

[a] Biomaterials and Corrosion Laboratory, Department of Materials Science and Engineering, Tel-Aviv University, Ramat Aviv, Tel Aviv 6997801, Israel
[b] School of Molecular Cell Biology and Biotechnology, Tel-Aviv University, Ramat Aviv, Tel Aviv 6997801, Israel

ARTICLE INFO

Keywords:
Circulating tumor cells (CTCs)
Bio-Ferrography (BF)
Atomic force microscopy (AFM)
Cancer cell elasticity
Adhesion
Young's modulus

ABSTRACT

Detecting the presence of circulating tumor cells (CTCs) in peripheral blood can be useful for monitoring treatment in patients, metastasis prognosis, and even early detection. The epidermal growth factor receptor (EGFR) is overexpressed in carcinoma, e.g. in colorectal cancer. Here, we use atomic force microscopy (AFM) force spectroscopy to study the mechanical properties of A431 cells, which simulate EGFR-overexpressing epithelial CTCs and were magnetically isolated by Bio-Ferrography (BF). BF is found useful in isolating individual cancerous cells for mechanical testing, thus avoiding cell-cell interactions. Different stages in the pre-isolation sample preparation steps (namely, cell fixation, PLL coating of the glass substrate, and immunomagnetic labeling) are found to affect the estimated Young's modulus. The BF magnetic isolation step itself does not change the elasticity of the captured cells in comparison to the pre-isolated microbeads-bound cells. The reported increase in the estimated Young's modulus between BF-isolated target cells and fixed cells that are not bound to magnetic microbeads can be used as a quantitative mechanical indicator for objective detection of CTCs. Furthermore, we report a 2.8-fold increase in the adhesion force between the AFM tip and the BF-isolated cells compared to the pre-isolated magnetic microbead-bound A431 fixed cells. This adhesion force correlation could potentially serve as an additional quantitative mechanical indicator for distinguishing between the target and background cells, without the use of cell staining assay and subjective analysis by an expert pathologist. This study demonstrates the powerful combination of the highly sensitive cell isolation by BF and the subsequent analysis of mechanical properties of individual captured cancerous cells by AFM. This combination has potential use in cancer research.

1. Introduction

The cytoskeleton is a complex network of protein filaments that play an important role in cell motility, cell division, structural support, and the mechanical properties of the cell (Alberts et al., 2002). The cytoskeletal network is comprised of three types of protein subunits which support the cellular membrane: actin microfilaments, intermediate filaments, and microtubules, all of which regularly change their organization during various cellular activities. Changes in the stiffness of individual cells can reveal significant information about the reorganization of these networks (Xu et al., 2012). These changes in cell stiffness can be quantified by the Young's modulus of elasticity, *E*.

The actin filaments have been reported to be the main factor dictating the mechanical properties of living cells. A high expression of actin, as observed in nonmalignant cells, is accompanied by a large value of Young's modulus. In contrast, lower expression of actin, observed in malignant cells, is associated with a lower Young's modulus (i.e. lower stiffness of the cell). Such measurements have been performed for various types of cells, such as ovarian (Xu et al., 2012), cervical (Zhao et al., 2015), and bladder (Ramos et al., 2014). It has been suggested that cell stiffness can serve as a potential biomarker for the detection of cancer-related alternations, and can potentially be used to define cancer diagnosis and monitoring criterion (Ramos et al., 2014). Several biomechanical assays have been used to study cell mechanics at the subcellular level, including optical tweezers, magnetic beads, micropipettes, etc. (Suresh, 2007). Nevertheless, the ability to control the lateral and vertical position of the atomic force microscope (AFM) tip, along with the loading force being controlled with high precision, have led to the AFM becoming one of the most versatile approaches in biomechanical cell research (Rianna and Radmacher, 2016; Haase and Pelling, 2015; Sokolov et al., 2013; Sokolov, 2007).

The Hertz contact model, which has been widely used to calculate

* Corresponding author.
E-mail address: neliaz@tau.ac.il (N. Eliaz).

https://doi.org/10.1016/j.jmbbm.2018.12.039
Received 3 April 2018; Received in revised form 26 December 2018; Accepted 30 December 2018
Available online 31 December 2018
1751-6161/

the Young's modulus of biological cells based on spherical indenters (and is also used in the present study), describes the stresses arising from the contact between two elastic spheres of different radii. This model is based on the following assumptions (Dintwa et al., 2008; Kuznetsova et al., 2007; Johnson and Johnson, 1987): (1) The material of the contacting bodies is isotropic, homogeneous and linearly elastic, namely it is represented by the Hooke's law; (2) The applied load is considered to be static; (3) The contacting surfaces are considered to be frictionless; (4) The indentation depth, δ, is small compared to the radius of the indented sphere, R ($\delta < 0.3R$) (Kuznetsova et al., 2007); and (5) The deformations are small, i.e. less than 10% sample thickness (nonlinearities that arise due to large deformations are not considered).

In the case of biological cells, the assumptions of the Hertz model are not all valid. While the cell membrane can be considered isotropic, the interior of the cell is anisotropic due to intracellular organelles and cytoskeleton organization. Cells also have a highly heterogeneous membrane structures, such as glycocalyx and membrane protrusions, which may exhibit varying rigidity at different areas and might induce frictional effects. Therefore, one cannot describe the elastic behavior of biological cells with a single Young's modulus value, and the measured Young's modulus needs to be correlated with the actual indentation depth. One needs to carefully assess the lateral and vertical measured cell dimensions, and accordingly choose the appropriate probe size. This will eventually determine the maximal indentation depth that satisfies the controlled assumptions. It should also be noted that the analyzed value of the Young's modulus for biological cells cannot be regarded as an *absolute* value because of several uncertainties: (1) The effects of loading rate (Li et al., 2008), tip geometry (Lekka, 2016; Puricelli et al., 2015), medium composition (Nikkhah et al., 2011), substrate type (Lekka, 2016; Domke et al., 2000), cell fixation (Codan et al., 2013; Dokukin et al., 2013), etc.; (2) Data analysis methodology, e.g. contact point evaluation (Crick and Yin, 2007), indentation depth (Pogoda et al., 2012), etc.; (3) Heterogeneities on the surface and cytoskeleton arrangement of biological cells (Lekka, 2016); and (4) Cell population heterogeneity due to the fact that cultured cells or cells obtained from a living organism are not synchronized in their cell cycle. Therefore, the measured Young's modulus can only be used in comparison to results obtained under the same measurement conditions following identical sample preparation procedures. In order to avoid a potential debate, we shall refer to our results reported in this paper as measured *estimated* Young's modulus.

Several studies (Codan et al., 2013; Pogoda et al., 2012; Kuznetsova et al., 2007) have suggested carrying out the AFM measurements on fixed cells. Fixation of erythrocytes using 5% formalin has been reported to lead to a 10-fold increase in the Young's modulus when compared to living erythrocytes (Mozhanova et al., 2003). Other studies have shown an increase in stiffness of fixed cardio-myocyte cells by a factor of 16 compared to living cells (Shroff et al., 1995). Although both experiments used the same fixative at the same concentration, one can see significant differences in the level of change in elasticity. Therefore, it can be concluded that varying types of cells are affected differently by the same fixative. A recent study assessed the Young's modulus of two cell lines: mouse embryonic fibroblasts (3T3) and human epithelial cancer cells (SW-13) via AFM measurements (Codan et al., 2013). Both living and fixed cells (3.5% paraformaldehyde) were studied. It was found that, with substantial statistical data, one can find a correlation between the mechanical properties of living and fixed cells. Furthermore, while living cells exhibited variance of the Young's modulus with time out of physiological conditions, fixed SW13 cells, which were analyzed after one day or one month since fixation, showed no statistical difference in the stiffness.

Cross et al. (2007) reported a decrease of approximately 70% in the stiffness of metastatic lung, breast, and pancreas cancer cells that originated from body fluids, in comparison to healthy cells. It was reported that not only can the mechanical analysis distinguish between cancerous and healthy cells, but it can also trace abnormalities in the elastic properties of cells associated with disease progression and different metastatic potential.

Ferrography is a sensitive, non-destructive condition monitoring method, which is based on magnetic isolation of ferromagnetic and paramagnetic particles from liquids and their deposition onto a glass slide for further microscopic and chemical analysis (Eliaz and Hakshur, 2012; Seifert and Westcott, 1972). Bio-Ferrography (BF) is a recent modification of the traditional Ferrography, which was developed to allow magnetic isolation of target cells and tissues (Eliaz, 2017; Eliaz and Hakshur, 2012). This technique has been used for isolation of bone and cartilage particles from synovial fluids for early diagnosis of osteoarthritis (Eliaz, 2017; Hakshur et al., 2011; Mendel et al., 2010), and isolation of both polymeric and metallic wear particles from synovial fluids for either design or failure analysis of artificial hip joints (Elsner et al., 2011, 2010; Meyer et al., 2006). BF has also been used to isolate cancer cells, with very promising results (Levi et al., 2015, 2014; Turpen, 2000; Fang et al., 1999). Fang et al. (1999) used BF to isolate rare MCF-7 breast carcinoma cells from human peripheral leukocytes using anti-epithelial membrane antigen antibodies and a magnetic colloid as immunomagnetic (IM) labeling. It was shown that the morphology of the selectively captured cancer cells was well-preserved. Levi et al. (2014) used BF to separate epidermal growth factor receptor (EGFR) positive colorectal cancer cells (CRCs) from EGFR-negative noncancer cells. EGFR-positive cancer cells could be separated from either buffer (PBS) or human whole blood (HWB). The reported recovery values in that study were 78% from 1 mL PBS and 53% from 1 mL HWB, with a limit-of-detection of 30 and 100 target cells, respectively. Later (Levi et al., 2015), design of experiments (DOE) methodology was implemented to optimize the BF isolation procedure for the EGFR high-positive circulating tumor cells (CTCs) application. An outstanding recovery rate of as high as 97% was achieved in the isolation of a very small number of target cells (2–100) suspended in a small volume (1 mL) of HWB, in a reduced number of 34 experiments. A primary clinical investigation by the same group (unpublished data) was next performed on blood samples drawn from 44 cancer patients and three healthy donors. It was found that in 83% of the metastatic CRC patient samples, at least one CTC could be identified unambiguously using the optimized BF isolation procedure. These results position BF as one of the most efficient and promising technologies for cancer cell separation. Here, we further implement quantitative mechanical analysis for non-subjective characterization of the isolated cancerous cells.

CTCs have mainly been studied in terms of enumeration and morphological analysis as a guiding prognosis in metastatic cancer patients. While numerous studies have investigated the mechanical properties of cultured cancer cells by means of AFM as a biomarker for disease pathogenesis and metastases potential, *only few have focused on the mechanical properties of CTCs* (isolated using size-based filtration) (Osmulski et al., 2014; Chen et al., 2013). The emergence of BF as a means for isolation of CTCs from whole blood, with attributes such as high recovery rates and non-destructiveness of the captured cells, opens new possibilities for characterization and analysis of CTCs at the single cell level. Investigation of the mechanical properties of CTCs by means of AFM force spectroscopy can potentially track variations in the elastic properties of the isolated CTCs as a biomarker with disease pathogenesis, progression and different metastatic potential. The objective of the present work is thus to investigate the effects of different stages of the BF protocol on the mechanical properties of cancerous cells as measured by AFM force spectroscopy. The findings in this research can potentially pave the way for future sensitive characterization, diagnosis, monitoring and treatment of metastasis in patients in a hospital environment.

2. Experimental section

2.1. The A431 cell line

In this study, A431 epidermoid carcinoma cells were used, simulating EGFR-overexpressing epithelial CTCs. A431 cells express about one million sites per cell of EGFR molecules (Derer et al., 2012). The BF separation protocol was applied on A431 target cells in phosphate-buffered saline (PBS). The A431 target cells were used either as living cells with no fixation or fixed with 4% formaldehyde.

2.2. Antibodies and magnetic microbeads

The IM labeling model that was applied in this study is based on the overexpression of EGFR on the surface of CTCs (as well as on the A431 target cells) (Derer et al., 2012), the ability of EGFR to be bound by the EGFR specific antibodies, and the ability of anti-IgG microbeads to bind to the capture antibodies. The IM model that was applied for A431 cell isolation was introduced by Levi et al. (Levi et al., 2015, 2014). R-1 mouse anti-human EGFR antibody (Santa Cruz Biotechnology, Inc., Santa Cruz, CA; 0.2 mg/mL) was used as the capture antibody. MicroBeads conjugated to monoclonal rat-anti-mouse IgG 2a + b antibody (Miltenyi Biotec, Inc., Auburn, CA) were used for cell separation.

2.3. Sample preparation for AFM force spectroscopy experiments

2.3.1. A431 cell culture and maintenance

A431 cells were cultured in Dulbecco's Modified Eagle Medium (DMEM) supplemented with 10% fetal calf serum (FCS), 2 mM L-glutamine, 100 U/mL penicillin, 100 μg/mL streptomycin, and 12.5 U/mL nystatin (Biological Industries, Israel) in a humidified 5% CO_2 incubator at 37 °C, according to ATCC A431 cell line protocol. The cultured 431 cells were split 2–3 times a week for constant accessibility, and harvested from the cell culture dish for further sample preparation about 12–24 h before AFM experiments were conducted.

2.3.2. Living A431 cells

In order to study the mechanical properties of living cells, A431 cells were harvested, using pre-warmed 1 × trypsin–EDTA solution, about 12–24 h before force spectroscopy measurements were conducted. The suspended living cells were seeded on sterilized 35 mm glass bottom Petri dish, 20 mm Glass #0 (De-Groot, Israel), at a density of about (1–2) × 10^5 cells per glass. The cells remained in the incubator for 12–24 h to enable cell-substrate attachment with low confluent cell concentration, to allow tip indentation of individual cells. This could prevent cell-cell interactions that might add uncontrolled uncertainties to repeated experiments. The medium was replaced right before the indentation experiment with pre-warmed supplemented medium to clear any dead cells that loosely attached to the coverslip or floated in the medium, thus reducing the risk of tip contamination. The samples were kept in the incubator until AFM measurements were conducted.

2.3.3. Fixed A431 cells

Cell fixation can prevent significant changes in the mechanical properties of the cells during the following IM labeling and magnetic isolation stages. Cell fixation preserves the micro-architecture and structure of the cell, preserves the cell elasticity over time (Codan et al., 2013), and allows AFM measurements in a wide range of temperatures, culture media, and pH values (Grimm et al., 2014). However, as chemical fixation involves cross-linking of proteins in the cytoskeleton, forming intermolecular bridges and networks of linked antigens, it changes the mechanical behavior of the cells. Formaldehyde was chosen in this study as the most proper fixative matter due to its ability to preserve cells without promoting dehydration and porosity of the cell membrane (in contrast to alcohols such as ethanol, which are known for their rapid action and penetration into the cell, and their subsequent dehydration of the cell).

In the case study of fixed cells, A431 cells were prepared according to Section 2.3.1, followed by gentle wash with PBS to fully remove remaining medium. Fixation with 4% formaldehyde for 20 min was carried out at room temperature. After the formaldehyde incubation step, the Petri dish was washed twice with PBS for 5 min. Samples were maintained air-sealed and refrigerated (4 °C) until the AFM measurements were conducted.

2.3.4. Fixed A431 cells attached to a PLL-treated surface

In biological research there are several coatings of glass or plastic surfaces which lead to increased cell-substrate attachment, including collagen I and IV, fibronectin (Cooke et al., 2008), or Poly-L-Lysine (PLL). PLL surface treatment was chosen for this study because it is suitable for attachment of suspended fixed cells (whereas collagen and fibronectin are not). The mechanism of cell attachment to PLL-treated surfaces is based on electrostatic interactions between the negatively charged cellular membrane and the positively charged PLL-coated glass surface. Thus, the PLL attachment mechanism is not dependent on cell viability. PLL treatment has been reported to be effective in keeping the analyzed cells immobilized while exerting forces on them by AFM tips (Ebner et al., 2011; Colville et al., 2009).

To study fixed A431 cells cultured on a PLL-treated glass bottom, a PLL surface coating was applied on the sterilized bottom of a glass Petri dish prior to A431 cell culturing and fixation. The glass bottom was immersed with 0.01% w/v PLL solution (Sigma, 0.1 w/v% PLL, 1:10 diluted with deionized water) for five minutes. The PLL solution was then removed, followed by drying under clean atmosphere hood with laminar airflow for a few hours.

2.3.5. A431 suspended fixed cells attached to PLL-treated surface

In this type of AFM force spectroscopy experiments, A431 cells were harvested from the cell culture, and transferred to a 14 mL tube. The suspended cells were then fixed with 4% formaldehyde. The suspended fixed cells were then seeded onto PLL-treated glass bottom Petri dishes at a density of about (1–2) × 10^5 cells per glass. Samples were maintained air-sealed in refrigeration at 4 °C for up to 24 h, until AFM measurements were conducted.

2.3.6. Suspended A431 fixed cells bound to magnetic microbeads and attached to a PLL-treated surface

In order to investigate the effect of magnetic microbeads that were bound to A431 fixed cells on the estimated Young's modulus of the cells, an IM labeling procedure was conducted. A 2 mL Eppendorf tube was used for the IM model solution preparation (see Section 2.2). The tube was filled with 0.3 mL PBS and mixed with 3 μL EGFR-specific (R-1) mouse anti-human IgG antibody (0.2 mg/mL) and 11 μL Miltenyi rat-anti-mouse IgG antibody conjugated to microbeads. Next, it was incubated at 4 °C for 20 min. During the incubation time period, 9 × 10^3 A431 suspended fixed cells (Section 2.3.5) were added into a 2 mL Eppendorf tube filled with 0.6 mL PBS and kept at 4 °C until the cocktail (capture antibody + microbeads) incubation time was completed. Next, an IM cocktail suspension in 0.1 mL PBS was added to the cell solution, followed by manual gentle shaking of the solution. The solution was then incubated for 2 h at 20 °C on a rotating orbital shaker (100 rpm). After incubation, the solution was centrifuged and washed with PBS (repeated two times). The described procedure is equivalent to one flow channel in BF separation process (5 channels in total). The mixture was then seeded on a PLL-treated glass bottom Petri dish, and maintained air-sealed at 4 °C for up to 24 h, by then AFM measurements were conducted.

2.3.7. A431 fixed cells BF-isolated on PLL-treated surface

To study A431 fixed cells that were captured using the BF cell isolation procedure, cells were fixed as described in Section 2.3.5. In this case study, PBS was used as a flow medium. The BF isolation procedure

is described in Section 2.4. Following the BF isolation process, the samples were maintained air-sealed at 4 °C for up to 24 h, by then AFM measurements were conducted.

2.4. Bio-Ferrography isolation methodology

The Bio-Ferrograph 2100 from Guilfoyle, Inc. (Fig. S3A) is a benchtop cytometry-based instrument. It utilizes a magnetic field that has a maximal field strength across an interpolar gap, where the collection of magnetically susceptible particles takes place. Since the gradient of that field is maximal at the edges of the gap, two parallel deposition strips – primary and secondary – are formed (Fig. S3B), and a rectangular deposition band can be observed on the ferrogram even by naked eye. A very high magnetic flux density is established at the interpolar gap, 1.67 T in our case. The BF directs five sample volumes through a small chamber (capture cell) over a glass substratum on the magnetic gap. This type of configuration allowed simultaneous processing of five samples under identical flow and magnetic field conditions (Eliaz and Hakshur, 2012; Eliaz, 2017).

The isolation (optimized) procedure, which comprised of an IM labeling stage followed by BF isolation, was done as described by Levi et al. (2015). The capture Ab EGFR (R-1) mouse-anti-human IgG antibody was mixed with microbeads conjugated to monoclonal rat-anti-mouse IgG antibody and incubated at 4 °C for 20 min. 1 mL of PBS samples spiked with 9×10^3 A431 target cells were prepared. The samples were incubated with the cocktail suspension at 20 °C using an orbital shaker (100 rpm). Following the incubation time period, the solution was centrifuged and washed with PBS.

The isolation by BF was conducted as follows, using a desktop Bio-Ferrograph 2100 (Guilfoyle, Belmont, MA). All samples were washed before the BF separation and adjusted to a fixed volume of 2 mL with PBS. The BF separation process started by filling the capture cell and the reservoir with 0.55 mL PBS at a flow rate of 1 mL/min. This was followed by adding the sample with target cells to the reservoir, then isolating the target cells within the deposition band at a predefined flow rate of 0.021 mL/min. Finally, the chambers were washed with 0.1 mL of PBS at the same flow rate. The slide with the isolated cells (ferrogram) was separated from the BF and examined under an inverted microscope (Olympus IX71). The cells were now ready for AFM force spectroscopy measurements.

2.5. Atomic force microscopy methodology

AFM experiments were conducted using a NanoWizard-III Bio AFM (JPK Instruments, Berlin), mounted on an inverted optical microscope (Olympus IX81, Tokyo, Japan), which was placed on top of an anti-vibration table, at × 20 and × 50 magnifications. The AFM head enables closed-loop reproducible tip positioning. AFM force spectroscopy (contact) mode was used in all experiments. Commercial silicon nitride cantilevers coated with reflex gold for better laser reflectivity were used, with a nominal spring constant of 0.08 N/m and a length of 200 μm. Silicon dioxide spherical tips were used, with a nominal tip diameter of either 2 or 3.5 μm (Sqube, Germany). The spherical tip was a preferred probe geometry (compared to standard sharp-end probes) due to attributes such as (Puricelli et al., 2015): (1) more uniform stress and strain distribution (it reduces the applied stress that acts on the cell surface), (2) less surface and in-cell heterogeneities.

All experiments were conducted in liquid, where the liquid type was chosen according to the nature of the experiment (PBS for fixed cells, supplemented DMEM for living cells). To this aim, the AFM was equipped with a liquid cell setup. For experiments involving living cells, a temperature control system (JPK's Petri Dish Heater) was used, keeping the analyzed cells at near-physiological conditions (37 °C). Carbon dioxide was not controlled. In certain experiments, A431 cells were transfected to stably express a red (mCherry) fluorescent protein, thus enabling their observation by fluorescent microscopy.

Prior to each cell indentation experiment, a system calibration was performed. It is noted that due to fabrication variance, the mechanical properties (such as spring constant and resonant frequency) of different cantilevers might differ slightly, hence, calibration is essential. The calibration consisted of two stages – calibration in air and calibration in liquid. Calibration in air was performed to determine the exact spring constant of the cantilever using the thermal tune method, while calibration in liquid was performed in order to determine the cantilever deflection sensitivity, by deflecting the cantilever on a hard surface (where cells are not present). The cantilever sensitivity calibration enabled the conversion of voltage changes in the photodetector signal due to cantilever deflection into metric units. In order to obtain force values, the classical beam theory ($F = kd$, where k is the cantilever spring constant and d is the cantilever deflection) was employed.

All force-indentation curves were conducted on randomly chosen, well-immobilized, separated individual cells, to eliminate the possible effects of neighboring cells on the cytoskeleton organization. The position of the AFM probe on a cell is shown in Fig. S1 (Supplementary data). Loading parameters were as follows: approach velocity of 2 μm/s, piezo target height of 7.5 μm, z-length of 5 μm, extended speed equals 1 μm/s. In each case, a proper set-point loading force was determined prior to data acquisition in order to achieve the desired indentation depth. This was performed by acquiring a series of ascending values of set-point forces. To obtain an accurate position of the AFM tip over the areas of interest during force-indentation curve acquisition, an optical overlay calibration was performed over $100 \times 100\ \mu m^2$ area, with a $5 \times 5\ \mu m^2$ calibration grid.

In order to account for the inherently heterogeneous nature of each cell, the heterogeneity of the cell population, and the uncertainty in the exact location of the nucleus, a grid scan methodology was employed. This type of measurement methodology allowed the collection of extensive statistical data for each case study and for each analyzed cell. The grid size was set to a square of either $3 \times 3\ \mu m^2$ or $2 \times 2\ \mu m^2$ (depending on the shape of the examined cells), with 8×8 data acquisition points, which resulted in 64 force-indentation curves per cell (the number of analyzed cells in each condition is specified in Section 3).

All collected force–indentation curves were analyzed using JPKSPM Data Processing software ver. 5.0.81 (JPK, Germany), using the Hertz contact model. For each case study, force-indentation curves were collected using the batch processing mode. Only the extension force curves were processed for each indentation. In order to evaluate the contact point, where the force curves first cross the zero force line, zero baseline was carried out, followed by contact-point evaluation process. In order to determine the actual cell indentation depth, the tip-sample separation was calculated.

To estimate the elasticity of the examined cells, expressed by the estimated Young's modulus, the collected force-indentation curves were fitted with the Hertz contact model for spherical tips, taking into account the appropriate tip radius used (either 1 or 1.75 μm). The Poisson's ratio was taken as 0.5, which represents an incompressible, linearly elastic solid at small strains (Berdyyeva et al., 2004). The predefined indentation depth (either 300 or 500 nm) was obtained by fitting using the Hertz model, according to the tip radius used. Depending on the sample type, pre-measurement calibration of the necessary loading force that results in sufficient indentation depth for the specific cell population was performed. During the manual fit process, each force-indentation curve was manually examined, and curves that showed inappropriate behavior or invalid fit were excluded. Throughout this manuscript, the estimated Young's moduli are reported, and comparison is made only between results obtained under the same experimental conditions. Data which was acquired with different tip diameters is not compared. Table S1 (Supplementary data) summarizes the experimental conditions that have been used and reported by other researchers for construction of AFM force-indentation curves of healthy and cancer cells. This information is provided here for

comparison, and as a useful tool for interested users.

3. Results and discussion

The BF isolation of CTCs consists of multiple sample preparation steps, such as sample washing and IM labeling of the target cells, followed by 2 h incubation with the cocktail suspension at 20 °C, with additional sample maintenance under non-physiological conditions (at 4 °C), and then the isolation process itself. Each step potentially introduces significant physiological and morphological changes of the target cells, including considerable effects on the cytoskeleton network reorganization and nuclear fragmentation. These effects might result in significant changes in the mechanical properties of the target cells due to the high dependence of the cell elasticity on cytoskeleton organization.

3.1. A431 cell line elasticity changes due to fixation

In order to determine the effect of fixation, AFM force spectroscopy of individual cells was performed on both living and fixed A431 cells before the BF isolation stage. The force-indentation curves describe the mechanical response of the subjected cells to an applied load. Therefore, in order to extract quantitative distinction between the force curves of living and fixed cells, the Hertz contact model for a spherical indenter with 300 nm indentation depth was fitted, and the estimated Young's moduli of the two examined cell types were calculated.

Typical force-indentation curve (extension phase) and fitting curve for a selected fitting range are presented in Fig. 1. In this figure, the extension (red) curve reflects the measured data, the fitted (green) curve is the Hertz contact model fit to 300 nm, and the blue dash line shows the Hertz extrapolation. The Hertz model fit shows good agreement with the experimental data.

The Young's moduli for living (n_{cells} = 21, n_{curves} = 954) and fixed (n_{cells} = 16, n_{curves} = 600) A431 cells were determined by generating cell population distribution histograms (Fig. 2B and A, respectively), which represent the total force-indentation analyzed curves for each cell line. The analysis shows that for the living A431 cells, the mean estimated Young's modulus is 0.48 ± 0.17 kPa, while for the fixed A431 cells it is 1.62 ± 0.73 kPa (Fig. 3A and B, respectively). This approximately 3-fold increase in the estimated elastic modulus (stiffness) can be explained by the chemical fixation process, which results in

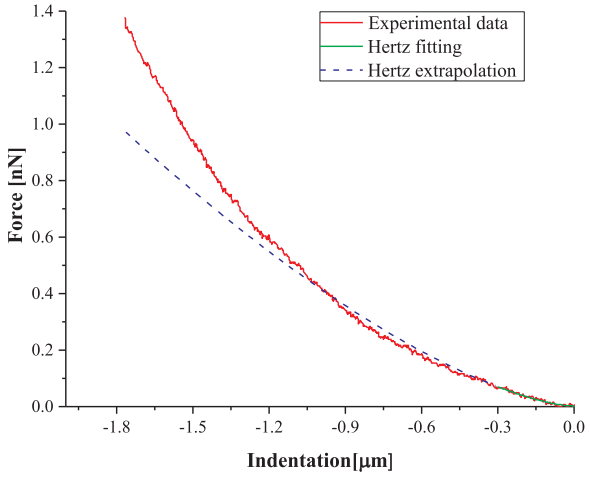

Fig. 1. Typical force–indentation for A431 living cells. Data curves showing the extension measured data (red line), the Hertz contact model fitting to 300 nm (green line), and the Hertz model extrapolation (blue dash line). The zero value on the *x*-axis represents the contact point. The negative values stem from the compression action of the indenter. (For interpretation of the references to color in this figure legend, the reader is referred to the web version of this article).

cross-linking of the cytoskeleton proteins in the interior of the cell and cross-linking of proteins on the cell membrane. The cross-linking forms intermolecular bridges, creating a network of linked antigens and, thus, changing the mechanical properties of the cell.

The estimated Young's modulus frequency histogram data is best represented by the lognormal distribution fitting. No adhesion between the AFM probe and the examined cells was observed for both living and fixed cells (in the order of magnitude of pN). Student's *t*-test ($p < 0.05$) showed a significant difference between the measured Young's moduli of the living and fixed cell cultures, with significant difference ($p < 0.05$) within the examined cell population.

3.2. A431 cell line elasticity changes due to substrate coating with PLL

The BF method involves isolation of magnetized target cells that are suspended in a liquid solution onto a coverslip slide. For further examination and analysis, for example by light or scanning electron microscopy or various staining assays, the captured cells are usually air-dried following the isolation process, which enables sufficient attachment of the cells to the substrate. However, for AFM force spectroscopy measurements, the examined cells should be fully immobilized onto the slide surface and maintained in an aqueous environment to avoid any membrane dehydration of the cells. In practice, suspended fixed cells do not allow sufficient adhesion to a non-treated glass substrate. In order to overcome this problem, PLL coating was applied onto the glass surface. But, it is known that the substrate's properties influence the organization of the cell cytoskeleton, thereby possibly affecting the mechanical properties of the cells. To evaluate this possible effect, AFM force spectroscopy mechanical analysis of individual A431 cells, cultured on a PLL-treated surface and then fixed by 4% formaldehyde, was conducted.

Throughout the AFM force spectroscopy analysis, the PLL surface coating facilitated sufficient adhesion between the target cells and the glass surface. The analyzed indentation curves were obtained and fitted using the Hertz contact model for a spherical indenter and an indentation depth of 300 nm. No adhesion between the AFM probe and the examined cells was observed (at a pN order of magnitude). The estimated Young's modulus was analyzed for 16 individual cells and a total of 1265 force-indentation curves. Thus, the population distribution histogram shown in Fig. 2C was generated. The mean and the standard deviation of the estimated Young's modulus were determined by fitting the frequency histogram data with the lognormal distribution fit. The analysis shows that for fixed A431 cell culture on a PLL-treated surface, the estimated Young's modulus is 2.68 ± 0.97 kPa. Student's *t*-test ($p < 0.05$) showed a significant difference of the estimated Young's modulus of fixed A431 cell population on a PLL-treated surface from fixed cell population on a PLL-untreated surface.

Comparing between A431 cell cultures on either PLL-treated or untreated substrates (Fig. 3B and C, respectively), PLL-coating of the substrate resulted in a 1.7-fold increase in the estimated Young's modulus. Student's *t*-test ($p < 0.05$) showed a significant difference ($p < 0.05$) between the measured estimated Young's modulus of fixed A431 cells on either PLL-treated or untreated surfaces. This increase is consistent with the results of Lekka (2016) who reported a 1.5-fold increase in the estimated Young's modulus between PLL-treated and untreated surfaces for HCV29 human bladder cells. It has been reported that PLL can induce membrane rearrangement with the formation of specific membrane deformation pattern within contact area (Kuznetsova et al., 2007). It was claimed that the elastic modulus values of cells adhered to extracellular matrix proteins that bind cells using integrins are higher compared to cells on glass and PLL that adhere the cells through nonspecific binding. The increase in the estimated Young's modulus due to PLL coating can be explained by the interaction between the cultured cells and the surrounding environment, namely the effect on the focal adhesion formation (Geiger et al., 2009) which causes reshaping of the cells, which in return results in difference in the

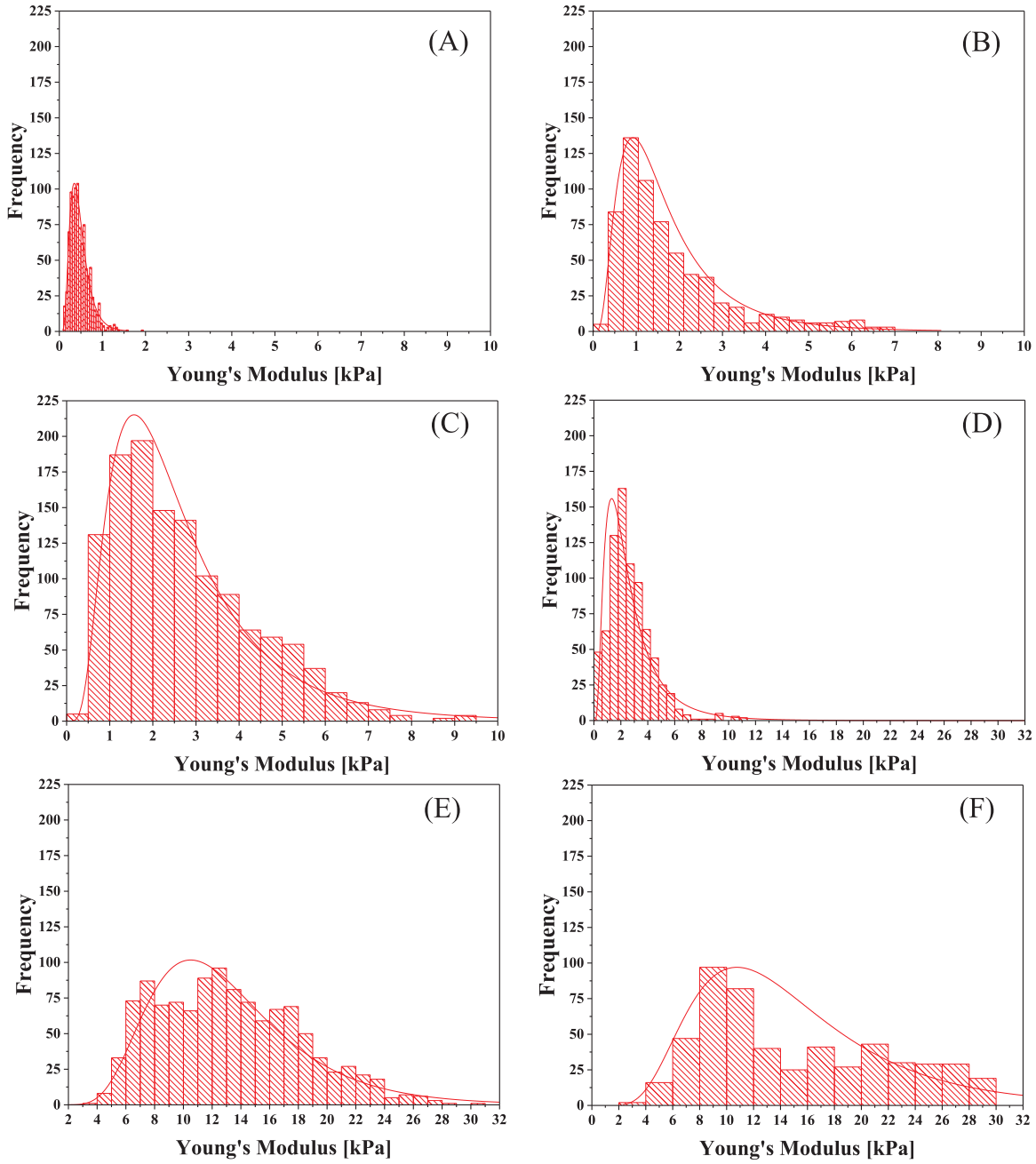

Fig. 2. Cell population histograms of the estimated Young's moduli with lognormal fitting. (A) Living A431 cells. (B) Fixed A431 cells. (C) A431 cells cultured on a PLL-coated surface followed by fixation. (D) Fixed (in suspension) A431 cells attached on a PLL-coated surface. (E) Fixed (in suspension) A431 cells bound to magnetic microbeads and suspended on a PLL-coated surface. (F) Fixed A431 cells after the BF isolation process.

cytoskeleton reorganization (mainly, the actin filaments network) (Rotsch and Radmacher, 2000) and in the elastic properties of the analyzed cells.

3.3. A431 cell line elasticity changes due to binding to magnetic microbeads

The BF isolation in this study is based on IM labeling of target cells which show high expression of EGFR on the membrane surface (such as A431 cells). The EGFR, which is present on the cell surface, is bound by EGFR specific antibody which is conjugated to anti-IgG MicroBeads (iron oxide nanoparticles with 50 nm nominal diameter). This procedure results in target cells that are bound to the microbeads and are ready to be isolated from the cell suspension using the BF method. The target cells are isolated from cell suspension onto a coverslip slide, where the captured cells are fixed. This does not allow sufficient adhesion to a non-treated glass substrate for proper AFM force spectroscopy tests. Therefore, PLL was used as a glass coating and showed sufficient adhesion of the target cells to the glass surface.

To investigate the induced mechanical changes of suspended A431 fixed cells due to binding to magnetic microbeads, AFM force spectroscopy mechanical analyses of individual cells were performed on two types of cell samples: (1) A431 fixed (in suspension) cells that were attached to a PLL-coated glass bottom Petri dish in PBS buffer solution; (2) as in (1), but the fixed cells were bound to magnetic microbeads prior to the attachment to the PLL-coated surface. Both cell samples showed sufficient adhesion to the PLL-coated surface throughout the AFM force spectroscopy tests.

For this set of comparative measurements, we used a probe with

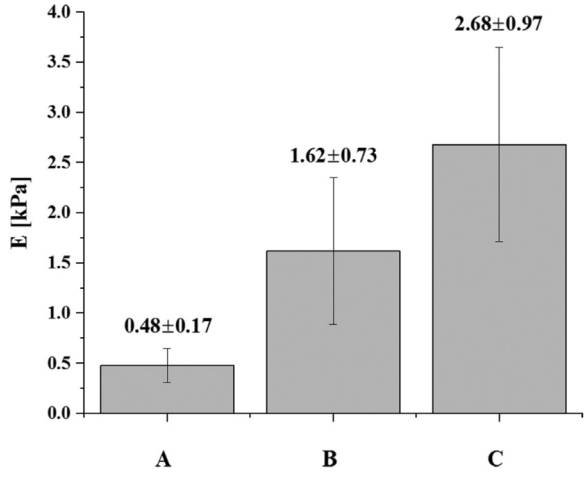

Fig. 3. Summary of the effect of different stages in the preparation of samples for BF isolation on the estimated Young's modulus of A431 cells. Error bars show the standard deviation from the mean value. A – living cells, B – fixed cells, C – fixed cell after PLL coating. All measurements were made with a nominal AFM tip diameter of 2 μm.

3.5 μm diameter, to increase the allowed indentation depth according to the Hertz contact model assumptions. The analyzed indentation curves were obtained and fitted using the Hertz model for an indentation depth of 500 nm. The estimated Young's modulus of the unbound cell sample was analyzed for 18 individual cells and 747 force-indentation curves in total, while for the magnetic microbead-bound cell samples the data was analyzed for 20 individual cells and 1138 force-indentation curves.

Using the estimated Young's modulus for each force-indentation curve, population distribution histograms were generated (Fig. 2D,E). The mean and the standard deviation of the estimated Young's modulus were calculated by fitting the frequency histogram data with the log-normal distribution fit. The analysis showed that the estimated Young's modulus of the unbound cells was 2.49 ± 0.81 kPa, while that of the magnetic microbead-bound cells was 13.2 ± 2.85 kPa. Student's *t*-test ($p < 0.05$) showed a significant difference between the Young's moduli of the two populations.

Comparing between the two cell populations (Fig. 4A and B), the magnetic microbead-bound cells show a 5-fold increase in the estimated Young's modulus. This increase in the estimated Young's modulus

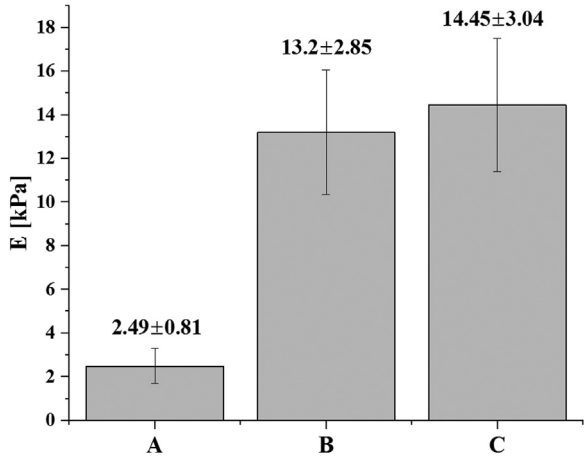

Fig. 4. Summary of the effect of different stages of the magnetic isolation itself on the estimated Young's modulus of A431 cells. Error bars show the standard deviation from the mean value. A – fixed cells in suspension, B – IM-labeled cells, C – BF-isolated cells. All measurements were made with a nominal AFM tip diameter of 3.5 μm.

clearly suggests that the magnetic beads-cell binding procedure results in cell coating with magnetic microbeads, which causes an increase in the apparent rigidity of the cells. As described in Section 2.3.6, the IM labeling procedure was performed using 50 nm microbeads made of an iron oxide core and a polymer shell. Iron oxide nanoparticles have been reported as having a Young's modulus of approximately 2.3 GPa (Guo et al., 2008). Thus, the beads used in this study are a few orders of magnitude stiffer than biological cells, and the binding of the analyzed cells to these microbeads can explain the significant increase in the measured estimated Young's modulus of microbead-bound cells.

Furthermore, comparison between the two histograms in Fig. 2D,E shows a significant increase in the histogram's full width at half maximum (FWHM), of approximately 4-fold, when the cells are bound to magnetic microbeads. This implies on significant increase in the variance in the measured value of the estimated Young's modulus. This phenomenon can be explained by the methodology of the force measurements (Section 2.5). The use of a spherical probe was based on the collection of data using a grid of force measurements approximately over the nucleus location. This methodology was chosen due to two reasons. Firstly, it was reported that prolonged indentation of cells in one location could result in reorganization of the cytoskeleton of single cells. Secondly, using solely an optical inverted microscope, even at a magnification of × 500, introduces uncertainty on whether the probe is placed exactly over the nucleus location, where the cell surface is relatively flat. To say, the measurements were taken in various places over the cell membrane surface. It is plausible that at each acquisition point, the density of the magnetic microbeads coating was different due to a non-homogenous dispersion of the EGFR receptor over the cell membrane (see Fig. S2), and consequently the measured stiffness may show increased variance for each individual cell. In addition, due to the probe scanning methodology discussed before, which results in indentation of certain overlapping contact areas of consequent data acquisition points, bead detachment or relocation over the examined cell membrane surface may occur. This can result in increased variance for each individual cell stiffness. In terms of the overall cell population, it is possible that due to the adsorption process of the cell suspension, the IM labeling procedure was not completely homogenous. This can result in different densities of bound magnetic microbeads within the labeled cell population, which will result in increased stiffness variance within a cell population.

Interestingly, in contrary to our previous report of low adhesion between the tip and the examined cells during the phase of AFM probe retraction (in the order of pN), in the case of A431 cells which had been bound to magnetic microbeads – an increase in the adhesion force between the silicon dioxide AFM probe and the magnetic microbead-bound cell was observed. The reason for this increase is not fully understood, yet several hypotheses can be ruled out: (1) Magnetic interactions between the AFM probe and the magnetic microbeads. This can be ruled out because the magnetic microbeads are made of an iron oxide superparamagnetic material, which results in zero apparent magnetic field when no external magnetic field is applied. (2) Electrostatic interactions between the AFM probe and the magnetic microbead-bound cells. This can be ruled out based on our measurements of the zeta potential of magnetic microbeads suspension in 1 mM KCl, which yielded a negative surface charge of the magnetic microbeads (–0.54 mV). In addition, it was reported that a silicon dioxide AFM probe with a nominal diameter of 2 μm also has a negative surface charge in 1 mM KCl (Barisik et al., 2014), thus adhesion due to electrostatic interaction can be ruled out. A typical force-indentation curve for a fixed A431 cell that had been bound to magnetic microbeads is presented in Fig. 5A. It illustrates the adhesion force between the AFM tip and the cell. The mean probe-cell adhesion force was analyzed for the retraction phase of the force-indentation curve for 20 individual cells and 1138 force-indentation curves. Thus, a population distribution histogram was generated (Fig. 5B). The mean and the standard deviation of the tip-cell adhesion were calculated by fitting the frequency

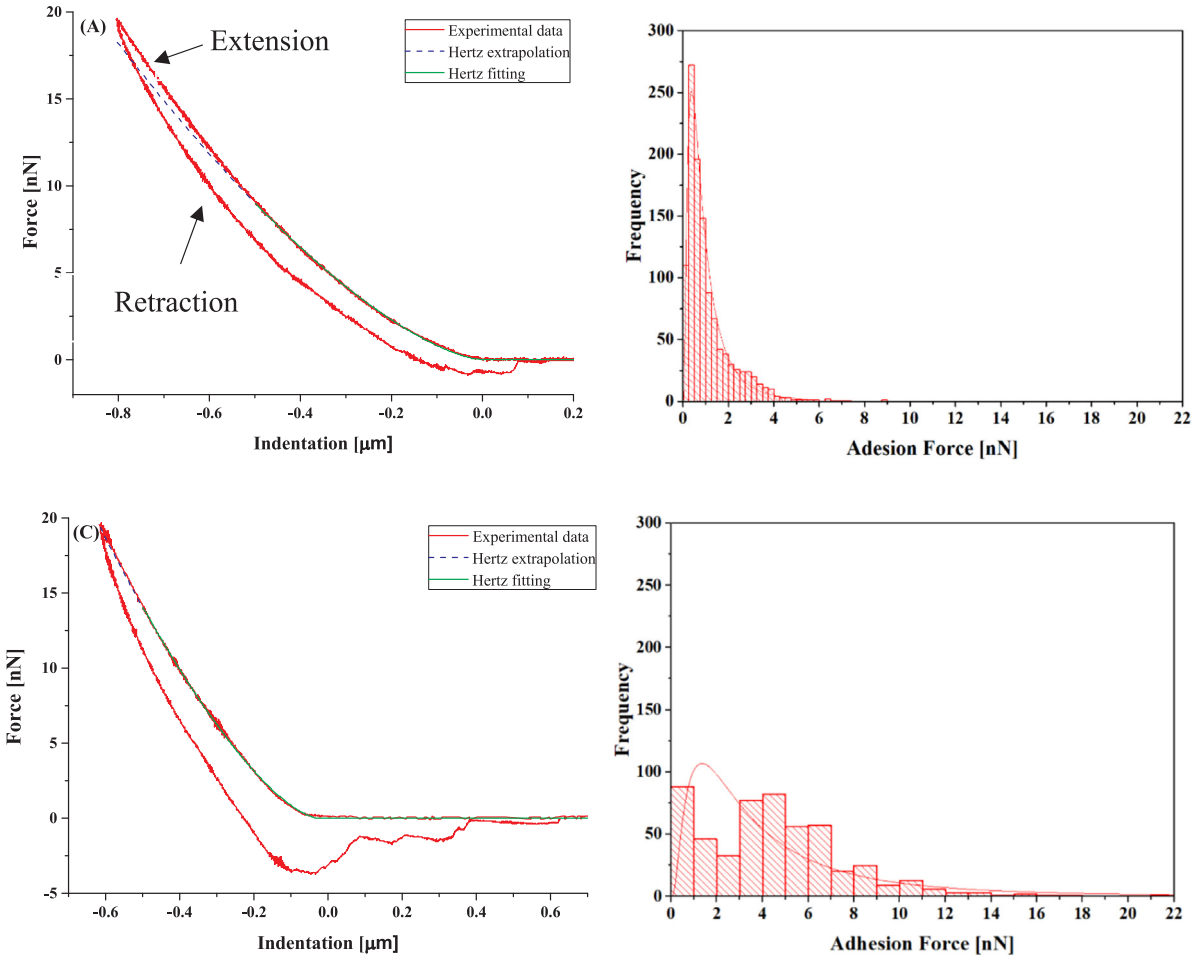

Fig. 5. (A) A typical force-indentation curve of magnetic microbead-bound fixed A431 cells on a PLL-treated glass surface (extension and retraction phases). (B) Cell population histogram of the obtained tip-cell adhesion force with lognormal fitting for A431 cells bound to magnetic microbeads. (C) A typical force-indentation curve for BF-isolated A431 fixed cells (extension and retraction phases). (D) A cell population histogram of the obtained tip-cell adhesion force with lognormal fitting for BF-isolated A431 cells.

histogram data with lognormal distribution. The analysis shows that for the cell samples that had been bound to magnetic microbeads, the adhesion force is 1.59 ± 0.72 nN.

3.4. A431 cell line elasticity changes due to BF isolation from PBS

Here, the mechanical properties of fixed (in suspension) A431 cells that had been captured using the BF protocol were investigated. The BF method requires magnetic labeling of the non-magnetic target cells, e.g. by IM with magnetic microbeads. In order to enable a proper comparison between the pre-isolated fixed A431 cells that had been bound to magnetic microbeads and the BF-isolated cells, the same preparation conditions were maintained, namely the same number of spiked target cells, IM labeling procedure, surface treatment with PLL, probe type, indentation depth, medium, etc. PBS served as the flow medium during the isolation process. The Hertz contact model was used to determine the estimated Young's modulus for 11 cells and 527 force-indentation curves in total. Determining the estimated Young's modulus for each force-indentation curve, a population distribution histogram was generated (Fig. 2F).

The analysis shows that for the cell samples that had been BF-isolated, the estimated Young's modulus is 14.45 ± 3.04 kPa. Student's *t*-test ($p < 0.05$) showed a significant difference between the estimated Young's moduli of the BF-isolated and magnetic microbead-bound pre-isolated cell populations.

Comparison between the two cell populations (Fig. 4B,C) revealed no effect of the BF isolation process on the elasticity of the captured cells. It is reasonable to assume that the variation between the two analyzed moduli (9% relative error) is due to the difference in the statistical data sample size (527 versus 1138 total analyzed force-distance curves for the BF-isolated cells and the microbeads-bound cells, respectively).

The increase in the estimated Young's modulus between BF-isolated target cells and fixed cells that had not been bound to magnetic microbeads can be used as a quantitative mechanical indicator for an objective detection of captured cells. This is a more efficient, more definite, more sensitive and less subjective way of analysis compared to the approach of H&E staining of the BF-isolated matter followed by morphological examination by an expert pathologist that we have used before. The identification of the isolated target cells originated in HWB is a challenging task for non-expert eyes, particularly due to the presence of mononuclear leukocytes, which might have been captured during the BF isolation process and form background noise, and their morphological resemblance to the isolated CTCs. The mononuclear leukocytes are magnetically captured most likely by a mechanism of non-specific binding to the magnetic microbeads. Nevertheless, it is plausible that the number of non-specific bound magnetic microbeads with the background leukocytes is significantly lower in comparison to the number of EGFR bonding sites that are present on the membrane surface of the target cells. All of these indicate that the magnetic bead binding process serves as an amplifier of the elastic modulus only for the target cells, and intensifies the signal-to-noise ratio between the

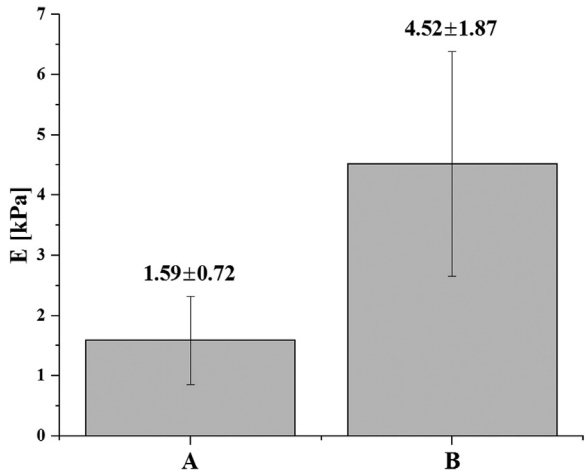

Fig. 6. Adhesion force population distribution of A431 fixed cells bound to magnetic beads and to a PLL-treated surface before (A) and after (B) the BF isolation process.

target cells and the background captured cells.

Interestingly, the cell sample population which had been isolated using BF in PBS medium showed two phenomena that were not observed in previous tests (see Sections 3.1–3.3). First, a substantial decrease in the adhesion between isolated A431 cells and the PLL-coated substrate is evident. This decrease affects the AFM force spectroscopy measurements due to cell mobilization as the probe indents into it, resulting in distorted and even unreliable force-indentation curves (see Fig. S4). Thus, cells that seemed to move based on light microscope observation or distorted data during the force measurement were excluded from the data analysis of the estimated Young's modulus. Our force spectroscopy experiments on BF-isolated A431 fixed cells showed a significant decrease in the adhesion between the cells and the surface in comparison to previous cases.

One assumption which can explain this phenomenon is that the BF-isolated cells were attached to the PLL-coated coverslip by the concentrated magnetic field, where the flow direction was in parallel to the substrate, in contrast to the other two cases of cell adhesion (namely, cells which had been cultured on the glass surface and cells which had been suspended and attached to the PLL-coated substrate by gravity). During the isolation process, the cells were exposed to a laminar flow regime (flow rate of 0.021 mL/min for approximately 3 h). The BF flow chamber can be considered as two parallel stationary plates. This configuration of two parallel stationary plates with laminar flow regime of the flow medium results in a maximal shear stress at the surface of the PLL-treated surface where the target cells are captured. It is plausible that during a long processing time and under the described flow regime with maximal shear stress profile at the PLL-cells interface, the adhesion efficiency of the isolated cells to the PLL-coated substrate decreased. This resulted in substantial difficulty in performing proper AFM force spectroscopy measurements. To confirm this hypothesis, further experiments need to be done (e.g. time/flow dependent experiments that would require changes in the BF protocol or identification of a better adhesive than PLL).

The second phenomenon that was observed for the BF-isolated cell samples was a 2.8-fold increase in the adhesion force between the spherical probe and the indented isolated cells during the retraction phase of the AFM probe, in comparison to the pre-isolated magnetic microbead-bound A431 fixed cells (Fig. 6). The analysis shows that for the isolated fixed A431 cells, the adhesion force is 4.52 ± 1.87 nN. This phenomenon, which occurred due to the BF isolation process, is not yet fully understood.

4. Conclusions

The present study offers insights into the mechanical properties of individual epithelial cancerous A431 cells that were isolated by Bio-Ferrography (BF) and studied by means of AFM force spectroscopy. Force-indentation curves were obtained and fitted using the Hertz contact model. BF was found useful in isolating individual cancerous cells for mechanical testing, thus avoiding cell-cell interactions. The mechanical properties analysis of the target cells was accomplished using a thorough examination of the dependent steps involved in the sample preparation and the BF isolation protocol. The examined pre-isolation sample preparation steps (namely, cell fixation, PLL coating of the glass substrate, and IM magnetic microbead labeling) were found to affect the measured estimated Young's modulus. A 3-fold increase in the stiffness of fixed cells compared to living cells was observed, which is attributed to cross-linking of the cytoskeleton proteins in the interior of the cell and cross-linking of proteins on the cell membrane. PLL-coating of the substrate was found to result in a 1.7-fold increase in the estimated Young's modulus, compared to an untreated substrate, which is explained by the interaction between the cultured cells and the surrounding environment. Magnetic microbead binding of cells led to a 5-fold increase in the estimated Young's modulus due to the higher rigidity of the bead coating on the cells. Yet, the BF magnetic isolation step itself did not change the elasticity of the captured cells in comparison to the pre-isolated microbeads-bound cells. The reported increase in the estimated Young's modulus between BF-isolated target cells and fixed cells that were not bound to magnetic microbeads can be used as a quantitative mechanical indicator for objective detection of CTCs. Furthermore, a 2.8-fold increase in the adhesion force between the AFM tip and the BF-isolated cells compared to the pre-isolated magnetic microbead-bound A431 fixed cells was found. This adhesion force correlation could potentially serve as an additional quantitative mechanical indicator for distinguishing between the target and background cells, without the use of cell staining assay and subjective analysis by an expert pathologist. The reported findings of this research pave the way for future detection and monitoring of metastasis in patients in a hospital environment. However, before this can happen, a standard operational protocol should first be established in order to make the comparison of results acquired in different laboratories possible. Next, we plan to carry out a comparative study of both healthy and cancerous cells isolated by BF from HWB by AFM force spectroscopy. In addition, we plan to conduct a clinical examination of patients at different stages of the cancer disease in an attempt to develop methodology for condition monitoring by BF-isolation of CTCs from HWB and subsequent AFM analysis.

Acknowledgments

We are grateful to Mr. Mario Levenstein, Dr. Limor Nahary, Dr. Assaf Shapira and Dr. Artium Khatchtouriants for their invaluable assistance.

Appendix A. Supplementary material

Supplementary data associated with this article can be found in the online version at doi:10.1016/j.jmbbm.2018.12.039.

References

Alberts, B., Johnson, A., Lewis, J., Raff, M., Roberts, K., Walter, P., 2002. The Cytoskeleton, Chapter 16. Molecular Biology of the Cell. Garland Science, New York.

Barisik, M., Atalay, S., Beskok, A., Qian, S., 2014. Size dependent surface charge properties of silica nanoparticles. J. Phys. Chem. C 118, 1836–1842.

Berdyyeva, T.K., Woodworth, C.D., Sokolov, I., 2004. Human epithelial cells increase their rigidity with ageing in vitro: direct measurements. Phys. Med. Biol. 50, 81.

Chen, C.L., Mahalingam, D., Osmulski, P., Jadhav, R.R., Wang, C.M., Leach, R.J., Chang, T.C., Weitman, S.D., Kumar, A.P., Sun, L., 2013. Single-cell analysis of circulating

tumor cells identifies cumulative expression patterns of EMT-related genes in metastatic prostate cancer. Prostate 73, 813–826.
Codan, B., Martinelli, V., Mestroni, L., Sbaizero, O., 2013. Atomic force microscopy of 3T3 and SW-13 cell lines: an investigation of cell elasticity changes due to fixation. Mater. Sci. Eng. C. 33, 3303–3308.
Colville, K., Tompkins, N., Rutenberg, A.D., Jericho, M.H., 2009. Effects of poly (L-lysine) substrates on attached Escherichia coli bacteria. Langmuir 26, 2639–2644.
Cooke, M., Phillips, S., Shah, D., Athey, D., Lakey, J., Przyborski, S., 2008. Enhanced cell attachment using a novel cell culture surface presenting functional domains from extracellular matrix proteins. Cytotechnology 56, 71–79.
Crick, S., Yin, F.C.-P., 2007. Assessing micromechanical properties of cells with atomic force microscopy: importance of the contact point. Biomech. Model. Mechanobiol. 6, 199–210.
Cross, S.E., Jin, Y.S., Rao, J., Gimzewski, J.K., 2007. Nanomechanical analysis of cells from cancer patients. Nat. Nanotechnol. 2, 780–783.
Derer, S., Bauer, P., Lohse, S., Scheel, A.H., Berger, S., Kellner, C., Peipp, M., Valerius, T., 2012. Impact of epidermal growth factor receptor (EGFR) cell surface expression levels on effector mechanisms of EGFR antibodies. J. Immunol. 189, 5230–5239.
Dintwa, E., Tijskens, E., Ramon, H., 2008. On the accuracy of the Hertz model to describe the normal contact of soft elastic spheres. Granul. Matter 10, 209–221.
Dokukin, M.E., Guz, N.V., Sokolov, I., 2013. Quantitative study of the elastic modulus of loosely attached cells in AFM indentation experiments. Biophys. J. 104, 2123–2131.
Domke, J., Dannöhl, S., Parak, W.J., Müller, O., Aicher, W.K., Radmacher, M., 2000. Substrate dependent differences in morphology and elasticity of living osteoblasts investigated by atomic force microscopy. Colloids Surf. B Biointerfaces 19, 367–379.
Ebner, A., Schillers, H., Hinterdorfer, P., 2011. Normal and pathological erythrocytes studied by atomic force microscopy. Chapter 15 in atomic force microscopy in biomedical research: methods and protocols. In: Braga, P.C., Ricci, D. (Eds.), Methods in Molecular Biology 736. Humana Press, pp. 223–241.
Eliaz, N., Hakshur, K., 2012. Fundamentals of tribology and the use of ferrography and bio-ferrography for monitoring the degradation of natural and artificial joints. In: Eliaz, N. (Ed.), Degradation of Implant Materials. Springer Science & Business Media, pp. 253–302.
Eliaz, N., 2017. Wear particle analysis, in ASM handbook. In: Totten, G.E. (Ed.), Friction, Lubrication, and Wear Technology 18. ASM International, Materials Park, OH, pp. 1010–1031.
Elsner, J.J., Mezape, Y., Hakshur, K., Shemesh, M., Linder-Ganz, E., Shterling, A., Eliaz, N., 2010. Wear rate evaluation of a novel polycarbonate-urethane cushion form bearing for artificial hip joints. Acta Biomater. 6, 4698–4707.
Elsner, J.J., Shemesh, M., Mezape, Y., Levenshtein, M., Hakshur, K., Shterling, A., Linder-Ganz, E., Eliaz, N., 2011. Long-term evaluation of a compliant cushion form acetabular bearing for hip joint replacement: a 20 million cycles wear simulation. J. Orthop. Res. 29, 1859–1866.
Fang, B., Zborowski, M., Moore, L.R., 1999. Detection of rare MCF-7 breast carcinoma cells from mixtures of human peripheral leukocytes by magnetic deposition analysis. Cytometry 36, 294–302.
Geiger, B., Spatz, J.P., Bershadsky, A.D., 2009. Environmental sensing through focal adhesions. Nat. Rev. Mol. Cell Biol. 10, 21–33.
Grimm, K.B., Oberleithner, H., Fels, J., 2014. Fixed endothelial cells exhibit physiologically relevant nanomechanics of the cortical actin web. Nanotechnology 25, 215101.
Guo, Z., Lei, K., Li, Y., Ng, H.W., Prikhodko, S., Hahn, H.T., 2008. Fabrication and characterization of iron oxide nanoparticles reinforced vinyl-ester resin nanocomposites. Compos. Sci. Technol. 68, 1513–1520.
Haase, K., Pelling, A.E., 2015. Investigating cell mechanics with atomic force microscopy. J. R. Soc. Interface 12, 20140970.
Hakshur, K., Benhar, I., Bar-Ziv, Y., Halperin, N., Segal, D., Eliaz, N., 2011. The effect of hyaluronan injections into human knees on the number of bone and cartilage wear particles captured by bio-ferrography. Acta Biomater. 7, 848–857.
Johnson, K.L., Johnson, K.L., 1987. Contact Mechanics. Cambridge University Press, UK.
Kuznetsova, T.G., Starodubtseva, M.N., Yegorenkov, N.I., Chizhik, S.A., Zhdanov, R.I., 2007. Atomic force microscopy probing of cell elasticity. Micron 38, 824–833.
Lekka, M., 2016. Discrimination between normal and cancerous cells using AFM. BioNanoScience 6, 65–80.
Levi, O., Shapira, A., Tal, B., Benhar, I., Eliaz, N., 2014. Isolating epidermal growth factor receptor overexpressing carcinoma cells from human whole blood by bio-ferrography. Cytom. Part B Clin. Cytom. 88, 136–144.
Levi, O., Tal, B., Hileli, S., Shapira, A., Benhar, I., Grabov, P., Eliaz, N., 2015. Optimization of EGFR high positive cell isolation procedure by design of experiments methodology. Cytom. Part B Clin. Cytom. 88, 338–347.
Li, Q.S., Lee, G.Y., Ong, C.N., Lim, C.T., 2008. AFM indentation study of breast cancer cells. Biochem. Biophys. Res. Commun. 374, 609–613.
Mendel, K., Eliaz, N., Benhar, I., Hendel, D., Halperin, N., 2010. Magnetic isolation of particles suspended in synovial fluid for diagnostics of natural joint chondropathies. Acta Biomater. 6, 4430–4438.
Meyer, D.M., Tillinghast, A., Hanumara, N.C., Franco, A., 2006. Bio-ferrography to capture and separate polyethylene wear debris from hip simulator fluid and compared with conventional filter method. J. Tribol. 128, 436–441.
Mozhanova, A., Nurgazizov, N., Bukharaev, A., 2003. Local elastic properties of biological materials studied by SFM. In: Proceedings of SPM-2003, pp. 2–5.
Nikkhah, M., Strobl, J.S., Schmelz, E.M., Agah, M., 2011. Evaluation of the influence of growth medium composition on cell elasticity. J. Biomech. 44, 762–766.
Osmulski, P., Mahalingam, D., Gaczynska, M.E., Liu, J., Huang, S., Horning, A.M., Wang, C.M., Thompson, I.M., Huang, T.H.M., Chen, C.L., 2014. Nanomechanical biomarkers of single circulating tumor cells for detection of castration resistant prostate cancer. Prostate 74, 1297–1307.
Pogoda, K., Jaczewska, J., Wiltowska-Zuber, J., Klymenko, O., Zuber, K., Fornal, M., Lekka, M., 2012. Depth-sensing analysis of cytoskeleton organization based on AFM data. Eur. Biophys. J. 41, 79–87.
Puricelli, L., Galluzzi, M., Schulte, C., Podestà, A., Milani, P., 2015. Nanomechanical and topographical imaging of living cells by atomic force microscopy with colloidal probes. Rev. Sci. Instrum. 86, 033705.
Ramos, J.R., Pabijan, J., Garcia, R., Lekka, M., 2014. The softening of human bladder cancer cells happens at an early stage of the malignancy process. Beilstein J. Nanotechnol. 5, 447–457.
Rianna, C., Radmacher, M., 2016. Cell mechanics as a marker for diseases: biomedical applications of AFM. AIP Conf. Proc. 1760, 020057.
Rotsch, C., Radmacher, M., 2000. Drug-induced changes of cytoskeletal structure and mechanics in fibroblasts: an atomic force microscopy study. Biophys. J. 78, 520–535.
Seifert, W., Westcott, V., 1972. A method for the study of wear particles in lubricating oil. Wear 21, 27–42.
Shroff, S.G., Saner, D.R., Lal, R., 1995. Dynamic micromechanical properties of cultured rat atrial myocytes measured by atomic force microscopy. Am. J. Physiol. Cell Physiol. 38, C286.
Sokolov, I., 2007. Atomic force microscopy in cancer cell research. Ch 1. In: Nalwa, H.S., Webster, T. (Eds.), Cancer Nanotechnology. American Scientific Publishers, pp. 1–17.
Sokolov, I., Dokukin, M.E., Guz, N.V., 2013. Method for quantitative measurements of the elastic modulus of biological cells in AFM indentation experiments. Methods 60, 202–213.
Suresh, S., 2007. Biomechanics and biophysics of cancer cells. Acta Mater. 55, 3989–4014.
Turpen, P., 2000. Isolation of cells using bioferrography. Cytometry (324-324).
Xu, W., Mezencev, R., Kim, B., Wang, L., McDonald, J., Sulchek, T., 2012. Cell stiffness is a biomarker of the metastatic potential of ovarian cancer cells. PLoS One 7, e46609.
Zhao, X., Zhong, Y., Ye, T., Wang, D., Mao, B., 2015. Discrimination between cervical cancer cells and normal cervical cells based on longitudinal elasticity using atomic force microscopy. Nanoscale Res. Lett. 10, 482.